RSC Advances

RSC Publishing

PAPER

View Article Online
View Journal

Optical stretching as a tool to investigate the mechanical properties of lipid bilayers†

Cite this: DOI: 10.1039/c3ra42510j

Mehmet E. Solmaz,[ab] Shalene Sankhagowit,[b] Roshni Biswas,[a] Camilo A. Mejia,[a] Michelle L. Povinelli[a] and Noah Malmstadt*[b]

Received 21st May 2013,
Accepted 9th July 2013

DOI: 10.1039/c3ra42510j

www.rsc.org/advances

Measurements of lipid bilayer bending moduli by various techniques produce widely divergent results. We attempt to resolve some of this ambiguity by measuring the bending modulus in a system that can rapidly process large numbers of samples, yielding population statistics. This system is based on optical stretching of giant unilamellar vesicles (GUVs) in a microfluidic dual-beam optical trap (DBOT). The microfluidic DBOT system is used here to measure three populations of GUVs with distinct lipid compositions. We find that gel-phase membranes are significantly stiffer than liquid-phase membranes, consistent with previous reports. We also find that the addition of cholesterol does not alter the bending modulus of membranes composed of a monounsaturated phospholipid.

Introduction

The elastic deformation of lipid bilayer membranes underlies many physiological processes such as enzyme activity modulation by the membrane[1] and mechanosensitive channel activity.[2] Membrane bending also governs the structural shape of vesicles,[3] membrane fusion processes,[4] and membrane-membrane interactions.[5] The bending elasticity of membranes can be described by three key parameters: spontaneous curvature (c_0), Gaussian modulus ($\bar{\kappa}$), and mean curvature modulus (or bending modulus, κ). For a symmetric bilayer, $c_0 = 0$, and $\bar{\kappa}$ can be ignored for topologically closed membranes.[6] The bending modulus therefore controls how much energy is required to bend a biomembrane. Accurate measurements of bending modulus are required for understanding the membrane contributions to the energetics of all of the processes in which membrane bending plays a role. Here we demonstrate a high-throughput method for quantitative measurement of bending modulus.

Giant unilamellar vesicles (GUVs), spherical structures with diameters in the range of 5–100 μm formed by a single lipid bilayer, represent a common model system for probing membrane mechanical properties.[7,8] GUVs have also been used to study the lipid raft hypothesis[9–11] and membrane transport processes.[12,13] Their large size relative to nanoscale liposomes allows for optical microscopy observations and manipulation of single vesicles. This facilitates a number of approaches to analyzing membrane mechanics.

The commonly implemented mechanical analysis techniques include vesicle fluctuation analysis,[7,14] electrodeformation,[15] and micropipette aspiration.[8,16] All operate on a single GUV. Vesicle fluctuation analysis determines the membrane bending modulus from analysis of subtle deformations in vesicle radii due to thermal fluctuations. The two-dimensional surface contours obtained at the equatorial plane of the vesicle are first decomposed into Fourier series. The bending modulus is obtained by fitting the experimentally obtained mean square amplitudes of the fluctuations to the theoretical amplitudes.[14,17] Electrodeformation subjects GUVs to AC electrical fields, in which they are elongated to ellipsoidal shapes.[18] The degree of deformation is dependent on the field intensity, frequency, medium conductivity, and the mechanical properties of the GUV. The measured apparent membrane area change and applied tension are used to deduce bending modulus values. In micropipette aspiration, suction pressure is applied through a micropipette on the GUV membrane, and the known tensions and measured apparent area changes yield both bending and area expansion modulus measurements.

There is variation in the bending modulus measurements obtained by the three primary methods described above, even when applied to the same lipid system.[19] For instance, the methods in which surface tension is applied using an external force (electrodeformation and micropipette aspiration) tend to give smaller κ values than vesicle fluctuation analysis. The dependence of measured bending modulus on the analytical technique was investigated recently by Niggemann *et al.*, who found different bending modulus values (14.3 ± 2.9 *vs.* $9.6 \pm 2.1kT$) using vesicle fluctuation analysis *vs.* electrodeformation on vesicles with identical lipid composition prepared in

[a]*Ming Hsieh Department of Electrical Engineering, University of Southern California, 3737 Watt Way, PHE 614, Los Angeles, CA 90089-0271, USA*
[b]*Mork Family Department of Chemical Engineering and Materials Science, University of Southern California, 925 Bloom Walk, HED 216, Los Angeles, CA 90089-1211, USA. E-mail: malmstad@usc.edu; Fax: +1 213 740 1056; Tel: +1 213 821 2034*
† Electronic supplementary information (ESI) available. See DOI: 10.1039/c3ra42510j

identical ways.[20] Vesicle fluctuation analysis studies on pure 1-palmitoyl-2-oleoyl-sn-*glycero*-3-phosphocholine (POPC) by two different groups resulted in different values (31.7 ± 1.0 *vs.* $38.5 \pm 0.8kT$).[21,22]

One shortcoming in the membrane mechanics literature has been a lack of robust statistical data derived from population analyses of ensembles of GUVs. Some studies have relied on measurements from one GUV per lipid composition.[23,24] Where populations have been studied, most studies have dealt with a small population of less than 10 GUVs.[7,15,20] while others analyzed between 10 and 20 GUVs.[25–27] Studies of large populations with careful statistical analysis have been rarer, with Faucon *et al.* studying 42 GUVs using fluctuation analysis[14] and Girard *et al.* investigating 85–90 GUVs with micropipette aspiration.[28]

A key advantage of the microfluidic dual-beam optical trap (DBOT)-based optical stretcher we present here is the ability to easily obtain population statistics. We have previously demonstrated the use of this tool to measure the bending modulus of a single GUV.[19] This tool can be used in a high-throughput mode: GUVs are flowed into a microfluidic channel. They are then captured and stretched one at a time in a stress-strain analysis protocol that takes less than 30 s per vesicle. Here, we apply this method to populations of GUVs to extract the bending modulus of membranes comprised of saturated and monounsaturated lipids in gel and liquid phases. We find that bending modulus values depend on lipid phase and are normally distributed for the three populations we tested. Our results also show that the addition of cholesterol to POPC membranes does not alter the bending modulus. This result contradicts reports that show increases in bending rigidity of POPC membranes with increasing cholesterol content.[22,29] However it is in agreement with the other recent reports that the bending moduli of unsaturated lipid membranes are independent of cholesterol concentration.[25,30] This technique is a promising route to obtaining statistically relevant bending modulus data for lipid membranes with controlled compositions.

Materials and methods

GUV preparation

1-Palmitoyl-2-oleoyl-sn-*glycero*-3-phosphocholine (POPC), 1,2-dipalmitoyl-sn-*glycero*-3-phosphocholine (DPPC), and cholesterol were purchased from Avanti Polar Lipids. Lipid mixtures of various composition were dissolved in chloroform and deposited onto an ITO-coated glass slide (Delta Technologies) for overnight vacuum drying. The resulting lipid film was rehydrated inside an electroformation chamber formed with two ITO-coated slides separated by a 2.5 mm-thick silicone spacer. This chamber was filled with a solution of 500 mM sucrose in 20 mM HEPES buffer at pH 7.0. POPC and DPPC GUVs were formed at room temperature ($\sim$23 °C) and 60 °C respectively for 2 h by applying a 1.5 V AC field with a frequency of 10 Hz. The electroformation temperatures were chosen so that the lipids remain in the fluid phase.

To achieve the optical contrast required for GUV optical stretching, sucrose in the solution outside the GUV was replaced by glucose with three two-fold serial dilutions with 500 mM glucose in 20 mM HEPES buffer at pH 7.0, as described previously.[19] The refractive indices, as measured with a refractometer (Atago), of the pure sucrose and glucose solutions were 1.3575 ± 0.0003 and 1.3455 ± 0.0003 respectively. The refractive index of the diluted GUV suspension was 1.3470 ± 0.0003.

Optical stretching

GUVs were flowed through a square glass microcapillary (Polymicro Technologies) that was connected to microfluidic adapters obtained from IDEX Health & Science. A diagram of the DBOT apparatus is shown in Fig. 1a. GUVs (green) in the fluidic channel (gray) assume a spheroidal shape when trapped due to the optical beams from two optical fibers (blue) facing each other. Flow was achieved using a peristaltic pump (P720/10 K) from Instech Laboratories, Inc. As a GUV approached the optical trap site, the flow speed was gradually decreased; flow was stopped completely when the GUV arrived at the trap site using a shut-off valve. The GUVs were visually inspected for defects/bilamellarity and only GUVs with clear surface fluctuations were selected for stretching. Trapping was achieved with minimal optical power (50 mW) from two identical diode lasers (LU0808M200) purchased from Lumics GmbH with optical fibers already end-coupled. The diodes were driven by current controllers (ITC 4005) obtained from Thorlabs. If the GUV was trapped off-center, it was brought to the midpoint of the flow channel, where the two optical beams were equal in power and size, by increasing the optical power from one of the fibers. We have analyzed potential errors arising from imprecise centering of the vesicles, and have found them to be insignificant (see ESI†). Stretching was done by gradually increasing each laser power to 250 mW in 11 steps with a holding time of 1 s at each step. Vesicle eccentricity increased with increasing laser power (Fig. 1b–c). Videos for each GUV were recorded at 61–67 fps using a GiGe camera from Basler AG.

Physical origin of stretching

To understand why the GUV stretches in a dual-beam trap, first consider the surface force on the GUV due to a single beam. A light ray incident on the front surface is partially reflected and partially transmitted. The surface force is proportional to the momentum change at the surface, $\Delta\overrightarrow{p} = \overrightarrow{p_i} - (\overrightarrow{p_r} + \overrightarrow{p_t})$, where $\overrightarrow{p_i}$, $\overrightarrow{p_r}$, and $\overrightarrow{p_t}$ are the momenta of the incident, reflected, and transmitted rays, respectively. The magnitude of the incident ray $p_i = n_iE/c$, where n_i is the refractive index outside the GUV, E is the photon energy, and c is the speed of light. For a given direction of incident light, $\overrightarrow{p_r}$ and $\overrightarrow{p_t}$ can be determined using Snell's Law and the Fresnel formulae. Assuming that the interior of the GUV has a refractive index greater than that of the exterior, the force on the front surface is negative and pulls the membrane back towards the beam source. The transmitted ray travels through the GUV to the back surface, where it is again partially reflected and partially transmitted. On the back surface, the force pushes the membrane in the beam direction. When two

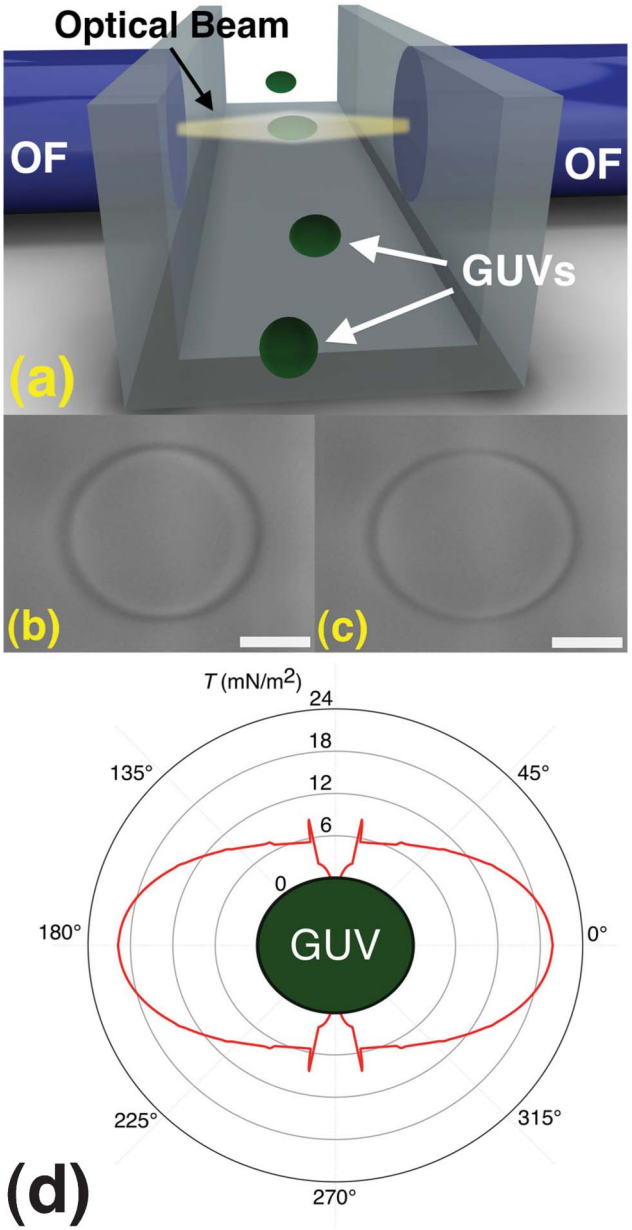

Fig. 1 Schematic illustration and mechanism of GUV trapping and stretching: (a) schematic of dual-beam optical fiber sources integrated with a microfluidic channel. Optical images of a GUV when (b) it is trapped with minimal power and showing slight eccentricity, and (c) when it is further stretched at maximum power. The scale bar is 10 μm. (d) The surface stress profile on the spheroidal GUV calculated using the ray optics method. The stress (T) at the poles (90° and 270°) is zero, while the maximum stress is at the equator or on the optical axis. The optical power from each beam is 50 mW.

beams are combined, their contributions to the force add. The net result is that while the total force on the GUV is zero at the center of the trap, the surface forces are non-zero and stretch the GUV along the beam axis.[31]

Data analysis

In the low-tension or fluctuation-dominated regime, the bending modulus (κ) of a lipid bilayer membrane is inversely proportional to the slope of apparent area strain *versus* natural log of membrane lateral tension.[8] During stretching, a GUV goes through axial deformation and assumes a more eccentric ellipsoidal shape. 2D contours of the vesicle boundary in the equatorial plane were traced from each video frame using MATLAB running in-house image processing software. The contours we obtain include surface fluctuations, and each contour from each video frame was decomposed as the radius of an equivalent volume sphere plus a sum of Legendre polynomials (see ESI†). We then use the second Legendre coefficient to get the apparent area strain associated with gross shape change.[25] The area strain values at each power level were recorded for 1 s of video. Since the GUVs included in the analysis reach steady-state deformation after ~200 ms (see ESI†), the average area strain was obtained from measurements taken during the final 500 ms of each hold step.

The homogeneous lateral surface tension (σ_h) was then calculated. After each increase in optical power, the GUV reaches an equilibrium shape with a homogeneous surface tension in the membrane. The pressure difference created inside (Δp) is equal on the equator and the poles of the ellipsoid. There is no applied stress at the poles. We can use the Young–Laplace equation to write

$$\Delta p = (c_1 + c_2)_{equ}\sigma_h - T_{equ} = (c_1 + c_2)_{pol}\sigma_h \quad (1)$$

where c_1 and c_2 are the principal curvature values at both the equator and the poles, and T_{equ} is the magnitude of stress exerted on the surface at the equator. We calculated the curvatures from the extracted contours. The optical stress T_{equ} was calculated using ray optics,[32] and an example is shown in Fig. 1d. Note that the surface stress is zero at the poles and the symmetrical discontinuities or spikes in the stress profile around the poles are a result of multiple internal reflections.[33,34] In our calculation, we included the effects of multiple bounces (up to 5) of each incident ray inside the GUV. For the refractive indices of the interior and exterior of the GUV used in our experiment, the reflection is small (R = 0.002%). We also performed calibration experiments to verify our optical force calculations. In these experiments, a polystyrene bead was pushed across the channel with a single laser beam.[35] Force was measured by assuming terminal velocity was achieved and setting drag force on the bead equal to applied optical force. The drag calculation was corrected for proximity of fluidic channel boundaries[36] and slip boundary conditions.[37] We observed that our theoretical optical force model was consistent with these force measurements. See the ESI† for a full description of these experiments. After finding the area strain and lateral tension values, we performed linear regression fitting to find κ and initial tension (*i.e.* tension on the membrane at zero applied optical force, σ_0). The fits with coefficient of determination (R^2) less than 0.7 were discarded.

Results and discussion

We first demonstrated that optical stretching is able to measure the difference in bending modulus of lipid mem-

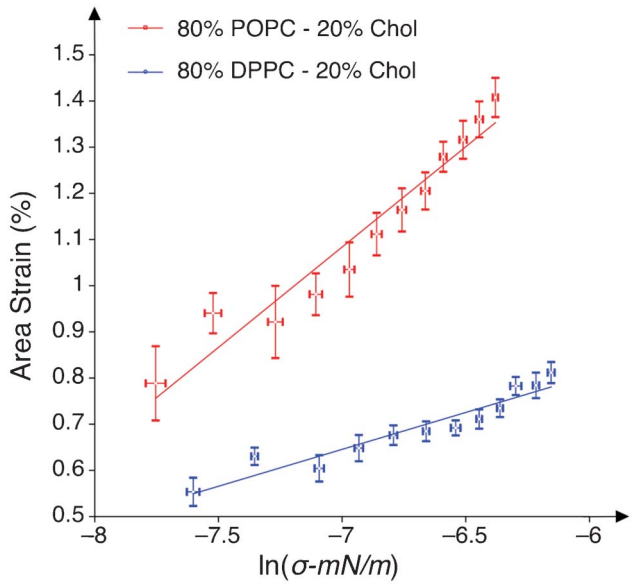

Fig. 2 Apparent area strain *versus* ln(tension) plots for POPC and DPPC GUVs with 20% cholesterol. The POPC lipid membrane is more flexible than DPPC lipid membrane. The error bars represent one standard deviation of area strain and lateral tension. The errors in bending modulus values are calculated from the standard errors of the slope using linear regression analysis.

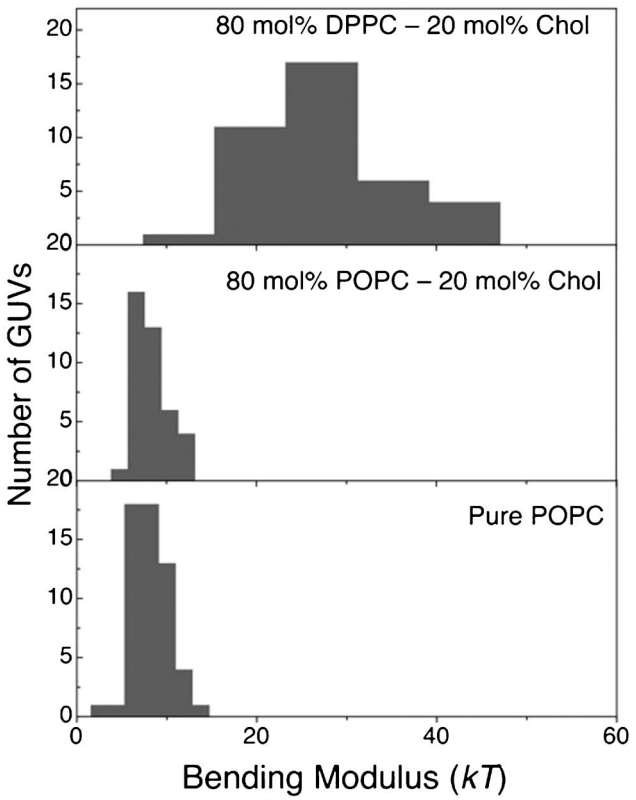

Fig. 3 Histograms of the bending modulus distributions of DPPC-Chol, POPC-Chol, and pure POPC lipid GUVs. Normal fits to these data for the three systems give bending moduli of 27.24 ± 7.69*kT*, 8.50 ± 1.83*kT*, and 8.13 ± 2.06*kT* respectively.

branes with different phase states. The bending modulus scales with membrane thickness squared multiplied by the area compressibility modulus ($\kappa \sim h^2 K_a$).[38] Gel-phase bilayers are thicker,[39] and the bending modulus of a lipid bilayer in the gel phase is consequentially higher than that of the same membrane in the liquid phase.[40,41] Under experimental conditions (at room temperature), both pure POPC and POPC with 20 mol% cholesterol are in the liquid phase whereas DPPC with 20 mol% cholesterol is in the gel phase.[42] Fig. 2 presents the dependence of relative area strain on applied tension for two GUV compositions: POPC and DPPC with 20 mol% cholesterol. We fit the formula $\Delta A/A = (kT/8\pi\kappa)\ln(\sigma_h/\sigma_0)$ to data plotted as area strain against induced surface tension.[8] We found σ_0 by extrapolating to the tension at zero area strain and κ by calculating the slope from the least-squares fit. For the two vesicles shown in Fig. 2, the initial tensions are at 7.53 ± 0.73 × 10^{-5} mN m^{-1} and 1.61 ± 0.19 × 10^{-5} mN m^{-1}, and the calculated bending modulus values are 9.16 ± 0.72*kT* and 24.89 ± 2.47*kT* for the POPC and DPPC membrane respectively.

To obtain population statistics, we measured the bending moduli of GUVs fabricated from pure POPC (n = 56), POPC with 20 mol% cholesterol (n = 40), and DPPC with 20 mol% cholesterol (n = 39) respectively. We were unable to produce high yields of pure DPPC GUVs. We fit normal distributions to the data to obtain the following bending modulus means and standard deviations: 8.13 ± 2.06*kT* for POPC vesicles, 8.50 ± 1.83*kT* for POPC with 20% Chol, and 27.24 ± 7.69*kT* for DPPC with 20% Chol. Histograms of the population bending modulus data are shown in Fig. 3.

We confirmed the normality of the population data using the Kolmogorov–Smirnov test. We then performed the student's t-test to compare the two POPC populations (POPC and POPC-20% Chol). The populations are not significantly different ($p > 0.05$). This analysis confirmed the indistinguishability of POPC populations with and without cholesterol, in contrast to other published results.[22,29] Cholesterol is believed to increase κ by ordering the acyl chains. Marsh did an extensive comparison of several methods and concluded that cholesterol increases mean bending moduli.[43] However recent reports have argued that the contribution of cholesterol to bending modulus is not universal and unsaturated lipids (particularly 1,2-dioleoyl-sn-*glycero*-3-phosphocholine, DOPC) are not affected by the addition of cholesterol.[25,30] Our results agree with these recent reports.

While the values of bending modulus that we have measured here are within the range of literature values,[15] they are near the minimum of this range. This may be due in part to the high concentrations (500 mM) of sugar used in these experiments. Work by Mitov and coworkers has shown that the bending modulus of membranes containing lipids with a single unsaturated tail can decrease significantly at elevated sucrose concentrations up to 400 mM.[44,45] Shchelokovskyy and coworkers have also found that sucrose/glucose concentrations in the range of 200 mM can significantly decrease the

bending modulus of membranes made from doubly unsaturated lipids.[46] These high sugar concentrations facilitated the relatively high index gradient between vesicle interior and exterior that made trapping and stretching possible.

There are several factors that may influence the width of the distributions shown in Fig. 3. GUVs made from POPC may be photooxidized when exposed to bright light during microscopy.[47] However, in our optical stretching experiment, the experimental duration for a single GUV was around 30 s, and no fluorescent dye was used, so we do not expect significant photooxidation to occur. The width of the DPPC/cholesterol distribution may also be a result of compositional heterogeneity due to non-uniform cholesterol incorporation during lipid film rehydration, as has been observed previously.[48]

We analyzed possible sources of systemic error in this experiment. One potential error source comes from how we calculated vesicle surface area, by fitting the contour shape as an expansion of spherical harmonics. For the data presented in Fig. 3, only the second Legendre coefficient is used to calculate the area change. When we include the fourth mode, as suggested in by Gracia and coworkers,[25] the bending modulus values tend to decrease by approximately 5%, within the reported error. Including the fourth mode does not decrease the width of the population histograms, indicating that lack of precision in shape fitting is not a major contributor to the width of the observed distributions.

Second, GUVs are trapped at a position slightly below the axis of the optical trap due to gravity. For example, consider a spheroidal GUV with 10 μm equivalent sphere diameter and eccentricity of 0.4. The net gravitational force on the GUV is proportional to the density difference between the solutions on the inside and outside and equals ~1.3 pN. The trapping position can be calculated by balancing the gravitational force with the optical gradient force. At the minimum trapping power of 100 mW, the GUV is trapped ~2 μm below the optical axis. At a power of 500 mW, the offset decreases to ~0.4 μm. The microscope is initially focused on the equatorial plane of the GUV. As the GUV is pulled further upward into the trap, the segment of the vesicle in the focal plane will shift.

To test whether this effect could have a significant impact on the results, we calculated the volume of the GUV at every frame by assuming the captured contour corresponded to the equatorial plane of a spheroidal vesicle and measuring the length of the major and minor axes. If the upward shift of the GUV were significant, it would be expected to result in consistently smaller measured GUV volumes as power increased. This is because the true volume of the GUV (expected to remain constant through this experiment) can be calculated from the true equatorial plane contour measured when the microscope is initially focused at minimum trapping power. Contours corresponding to other GUV cross-sections would result in a smaller calculated volume. A significant shift of the vesicle along the optical axis would therefore result in an

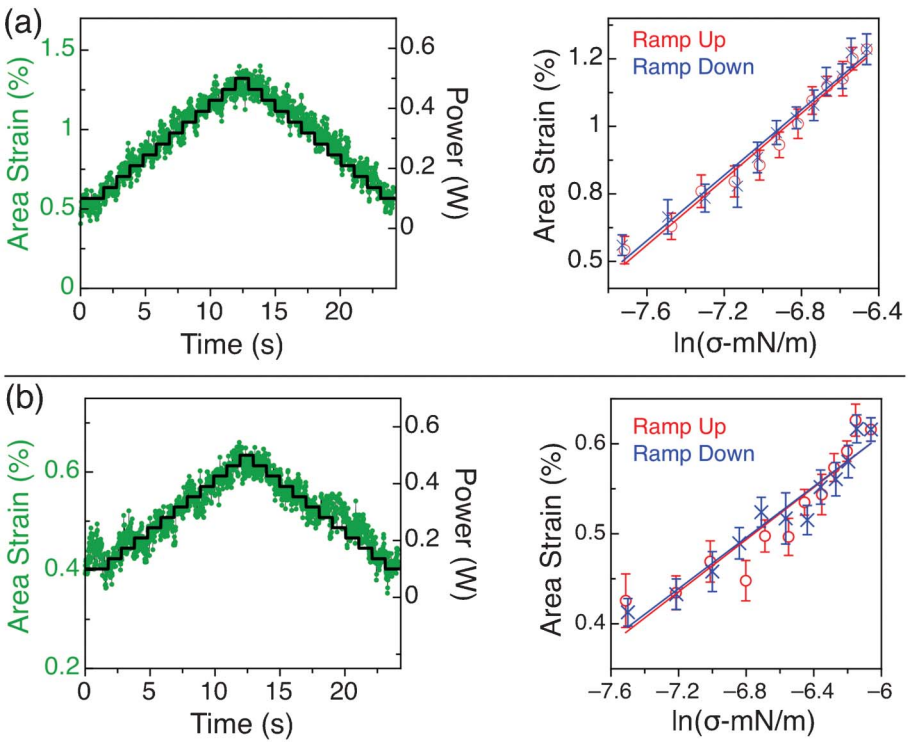

Fig. 4 Laser power ramp-up and ramp-down experiments on two different GUVs. Plots on the left show laser power (black) and vesicle area strain (green) as a function of time. Plots on the right show the calculated stress-strain relationship. We obtain two bending modulus values corresponding to ramp-up (κ) and ramp-down (κ') data. (a) POPC, $\kappa = 6.52 \pm 0.32kT$ and $\kappa' = 6.58 \pm 0.35kT$; (b) DPPC-20%Chol, $\kappa = 27.47 \pm 3.29kT$ and $\kappa' = 28.04 \pm 2.25kT$.

apparent (and purely artifactual) decrease in volume. In fact, in no experiment did the average calculated volume change exceed 1%, and there was no relationship between volume and power.

Finally, we performed a set of experiments to test whether the GUV stretching system exhibits hysteresis. The optical power was ramped up and down between minimum and maximum trapping power. The bending modulus was obtained both as the vesicle dilated and contracted. Fig. 4 shows two examples of time-dependent area strain and extracted area strain *vs.* surface tension, for pure POPC (Fig. 4a) and DPPC-20%Chol (Fig. 4b). For this POPC vesicle, the bending modulus values obtained from the two slopes gave 6.52 $\pm$ 0.32kT for ramp-up and 6.58 $\pm$ 0.35kT for ramp-down. For this DPPC-20%Chol vesicle, we obtained 27.47 $\pm$ 3.29kT for ramp-up and 28.04 $\pm$ 2.25kT for ramp-up and ramp-down. In all cases tested, the change in measured bending modulus for the two different deformation directions is within error.

It is well known that electroformation produces GUVs with highly variable σ_0.[49] Histograms of the initial tension values measured for all three populations of GUVs are included in the ESI.† Fig. 5 shows an example of two GUVs with similar κ but σ_0 differing by nearly four orders of magnitude. In fact we regularly observed that very different values of σ_0 could correspond to similar values of κ. Our analysis indicated that κ and σ_0 are, if anything, only weakly correlated.

The breadth of the κ distributions may be the result of significant structural differences between the various GUVs. Helfrich has argued that microscale membrane ''superstructures'' could induce unusual tension behavior,[50] and so-called ''hidden reservoirs'' of lipids in GUVs have been found to cause variability in other optical-force experiments.[51] Variability could be reduced by developing a GUV fabrication method that allows for better tension state control than electroformation or by implementing an objective and automatable set of criteria for selecting vesicles restricted to a limited range of initial tensions.

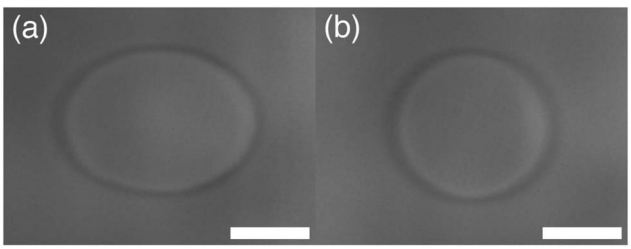

Fig. 5 Two pure POPC vesicles showing similar bending moduli corresponding to very different initial tensions. These images show the vesicle stretch at maximum optical power. (a) κ = 10.62 $\pm$ 1.06 kT and σ_0 = 4.36 $\times$ 10^{-8} mN m^{-1}; (b) κ = 9.80 $\pm$ 0.90 kT and σ_0 = 2.51 $\times$ 10^{-4} mN m^{-1}. Scale bars are 10 μm.

Conclusions

In conclusion, we have used optical stretching in a microfluidic DBOT system to investigate the elastic bending modulus of populations of GUVs composed of POPC, POPC with 20% Chol, and DPPC with 20% Chol. While the exact bending moduli measured here are particular to the aqueous solution conditions used (particularly ionic strength and sugar concentration), this approach provides a useful means for comparing mechanical properties across various lipid compositions at the same solution conditions. The difference in bending modulus between liquid and gel-phase GUVs is unambiguous; gel-phase GUVs are significantly stiffer. The bending elastic modulus of the membrane composed of the monounsaturated phospholipid (POPC) is insensitive to Chol at concentrations up to 20%. This technique is a simple and powerful approach to the measurement of membrane bending properties. It has the potential to be widely deployed in efforts to understand relationships between membrane composition and membrane mechanics.

Abbreviations

GUV	giant unilamellar vesicle
AC	alternating current
POPC	1-palmitoyl-2-oleoyl-sn-*glycero*-3-phosphocholine
DPPC	1,2-dipalmitoyl-sn-*glycero*-3-phosphocholine
ITO	indium-tin oxide
RO	ray optics
Chol	cholesterol

Acknowledgements

This work was supported by the Office of Naval Research (Young Investigator Award N00014-12-1-0620) and the National Institutes of Health (Award 1R01GM093279). Optical force calculations were supported by the National Science Foundation (CAREER Award 0846143). Optical device development was funded by the National Institutes of Health (Award 5U54CA143907).

References

1 G. S. Attard, R. H. Templer, W. S. Smith, A. N. Hunt and S. Jackowski, *Proc. Natl. Acad. Sci. U. S. A.*, 2000, **97**, 9032–9036.
2 E. Perozo, A. Kloda, D. M. Cortes and B. Martinac, *Nat. Struct. Biol.*, 2002, **9**, 696–703.
3 H. J. Deuling and W. Helfrich, *J. Phys.*, 1976, **37**, 1335–1345.
4 L. V. Chernomordik and M. M. Kozlov, *Nat. Struct. Mol. Biol.*, 2008, **15**, 675–683.
5 E. A. Evans and V. A. Parsegian, *Proc. Natl. Acad. Sci. U. S. A.*, 1986, **83**, 7132–7136.

6 W. Helfrich and R. Servuss, *Nuovo Cimento Soc. Ital. Fis., D*, 1984, **3**, 137–151.
7 H. Engelhardt, H. P. Duwe and E. Sackmann, *J. Phys., Lett.*, 1985, **46**, 395–400.
8 E. Evans and W. Rawicz, *Phys. Rev. Lett.*, 1990, **64**, 2094–2097.
9 L. A. Bagatolli and E. Gratton, *Biophys. J.*, 2000, **78**, 290–305.
10 C. Dietrich, L. A. Bagatolli, Z. N. Volovyk, N. L. Thompson, M. Levi, K. Jacobson and E. Gratton, *Biophys. J.*, 2001, **80**, 1417–1428.
11 S. L. Veatch and S. L. Keller, *Biophys. J.*, 2003, **85**, 3074–3083.
12 S. Li, P. C. Hu and N. Malmstadt, *Anal. Chem.*, 2010, **82**, 7766–7771.
13 S. Li, P. C. Hu and N. Malmstadt, *Biophys. J.*, 2011, **101**, 700–708.
14 J. Faucon, M. D. Mitov, P. Méléard, I. Bivas and P. Bothorel, *J. Phys.*, 1989, **50**, 2389–2414.
15 M. Kummrow and W. Helfrich, *Phys. Rev. A: At., Mol., Opt. Phys.*, 1991, **44**, 8356–8360.
16 E. Evans and D. Needham, *J. Phys. Chem.*, 1987, **91**, 4219–4228.
17 S. T. Milner and S. A. Safran, *Phys. Rev. A: At., Mol., Opt. Phys.*, 1987, **36**, 4371–4379.
18 R. Dimova, K. A. Riske, S. Aranda, N. Bezlyepkina, R. L. Knorr and R. Lipowsky, *Soft Matter*, 2007, **3**, 817–827.
19 M. E. Solmaz, R. Biswas, S. Sankhagowit, J. R. Thompson, C. A. Mejia, N. Malmstadt and M. L. Povinelli, *Biomed. Opt. Express*, 2012, **3**, 2419–2427.
20 G. Niggemann, M. Kummrow and W. Helfrich, *J. Phys. II*, 1995, **5**, 413–425.
21 H. Bouvrais, T. Pott, L. A. Bagatolli, J. H. Ipsen and P. Meleard, *Biochim. Biophys. Acta, Biomembr.*, 2010, **1798**, 1333–1337.
22 J. Henriksen, A. C. Rowat and J. H. Ipsen, *Eur. Biophys. J.*, 2004, **33**, 732–741.
23 P. Méléard, C. Gerbeaud, P. Bardusco, N. Jeandaine, M. D. Mitov and L. Fernandez-Puente, *Biochimie*, 1998, **80**, 401–413.
24 M. Kocun and A. Janshoff, *Small*, 2012, **8**, 847–851.
25 R. S. Gracia, N. Bezlyepkina, R. L. Knorr, R. Lipowsky and R. Dimova, *Soft Matter*, 2010, **6**, 1472–1482.
26 J. R. Henriksen and J. H. Ipsen, *Eur. Phys. J. E*, 2004, **14**, 149–167.
27 P. Méléard, T. Pott, H. Bouvrais and J. Ipsen, *Eur. Phys. J. E*, 2011, **34**, 1–14.
28 P. Girard, J. Prost and P. Bassereau, *Phys. Rev. Lett.*, 2005, **94**, 088102.
29 L. R. Arriaga, I. Lopez-Montero, F. Monroy, G. Orts-Gil, B. Farago and T. Hellweg, *Biophys. J.*, 2009, **96**, 3629–3637.
30 J. Pan, T. T. Mills, S. Tristram-Nagle and J. F. Nagle, *Phys. Rev. Lett.*, 2008, **100**, 198103.
31 J. Guck, R. Ananthakrishnan, T. J. Moon, C. C. Cunningham and J. Kas, *Phys. Rev. Lett.*, 2000, **84**, 5451–5454.
32 H. Sosa-Martinez and J. Gutierrez-Vega, *Proc. SPIE–Int. Soc. Opt. Eng.*, 2009, **7400**, 74002B.
33 A. E. Ekpenyong, C. L. Posey, J. L. Chaput, A. K. Burkart, M. M. Marquardt, T. J. Smith and M. G. Nichols, *Appl. Opt.*, 2009, **48**, 6344–6354.
34 P. B. Bareil, Y. L. Sheng and A. Chiou, *Opt. Express*, 2006, **14**, 12503–12509.
35 J. Guck, R. Ananthakrishnan, H. Mahmood, T. J. Moon, C. C. Cunningham and J. Kas, *Biophys. J.*, 2001, **81**, 767–784.
36 K. Svoboda and S. M. Block, *Annu. Rev. Biophys. Biomol. Struct.*, 1994, **23**, 247–285.
37 A. B. Basset, *A treatise on hydrodynamics with numerous examples*, Dover Publications, New York, 1961, p. 2 v.
38 E. A. Evans, *Biophys. J.*, 1974, **14**, 923–931.
39 J. F. Nagle and S. Tristram-Nagle, *Biochim. Biophys. Acta, Rev. Biomembr.*, 2000, **1469**, 159–195.
40 K. R. Mecke, T. Charitat and F. Graner, *Langmuir*, 2003, **19**, 2080–2087.
41 T. Heimburg, *Biochim. Biophys. Acta, Biomembr.*, 1998, **1415**, 147–162.
42 G. W. Feigenson and J. T. Buboltz, *Biophys. J.*, 2001, **80**, 2775–2788.
43 D. Marsh, *Chem. Phys. Lipids*, 2006, **144**, 146–159.
44 J. Genova, A. Zheliaskova and M. D. Mitov, *Colloids Surf., A*, 2006, **282**, 420–422.
45 V. Vitkova, J. Genova, M. D. Mitov and I. Bivas, *Mol. Cryst. Liq. Cryst.*, 2006, **449**, 95–106.
46 P. Shchelokovskyy, S. Tristram-Nagle and R. Dimova, *New J. Phys.*, 2011, **13**, 025004.
47 A. G. Ayuyan and F. S. Cohen, *Biophys. J.*, 2006, **91**, 2172–2183.
48 E. Baykal-Caglar, E. Hassan-Zadeh, B. Saremi and J. Huang, *Biochim. Biophys. Acta, Biomembr.*, 2012, **1818**, 2598–2604.
49 M. I. Angelova, N. Hristova and I. Tsoneva, *Eur. Biophys. J.*, 1999, **28**, 142–150.
50 W. Helfrich, Tension-induced mutual adhesion and a conjectured superstructure of lipid membranes, in *Handbook of Biological Physics*, ed. R. Lipowsky and E. Sackmann, Elsevier Science, Amsterdam, 1995, pp. 691–721.
51 G. Koster, M. VanDuijn, B. Hofs and M. Dogterom, *Proc. Natl. Acad. Sci. U. S. A.*, 2003, **100**, 15583–15588.